



Finite element modeling protocols and parametric analyses for short cold-formed steel zee-section beam-columns

Shahabeddin Torabian¹, Hamed Amouzegar², Mazdak Tootkaboni³, Benjamin W. Schafer⁴

Abstract

A modeling protocol for shell finite element modeling of cold-formed steel Zee-sections is proposed via a parametric study on specimens previously tested in an experimental study on cold-formed steel Zee-section beam-columns under bi-axial moments and axial force. The experimental dataset consists of twenty-two short Zee-section beam-columns with nominal 178 mm [7 in.] deep webs, 57 mm [2.25 in.] wide flanges 19.5 mm [0.766 in.] long lips at 48 deg. and a short member length of 305 mm [12 in.]. The numerical models include geometric and material nonlinear shell finite element collapse analyses in ABAQUS. The parameters include residual stresses and strains from roll-forming, geometrical dimensions, and geometric imperfection pattern and magnitude. The numerical results verify the experimentally observed high sensitivity of the Zee-sections to lip (local and/or distortional) buckling. The strength surface of the Zee-section beam-columns, generated numerically, exhibits regions where significantly more strength in cold-formed steel beam-columns is expected when compared to a linear interaction surface as adopted in the current design methods. The potential for further improvement of the current approach for predicting the strength of cold-formed steel beam-columns is discussed.

1. Introduction

Beam-columns require greater attention and calculation in analysis and design due to the interaction of the applied axial load and the bending moments. Current cold-formed steel design codes such as the North American Specification of the American Iron and Steel Institute (AISI-S100 2012), and the Australian/New Zealand Standard (AZ/NZS) for cold-formed steel structures (AS/NZS 2005) have adopted a linear interaction equation for combining the axial load and bending moments applied to beam-columns. In cold-formed steel design, the complexity in beam-columns is even more pronounced due to sensitivity of thin cross-section

¹ Assistant Research Professor, Department of Civil Engineering, Johns Hopkins University, <torabian@jhu.edu>
School of Civil Engineering, College of Engineering, University of Tehran, <torabian@ut.ac.ir>

² Graduate Student, Department of Civil and Environmental Engineering, University of Massachusetts, Dartmouth, <hamouzegar@umassd.edu>

³ Assistant Professor, Department of Civil and Environmental Engineering, University of Massachusetts, Dartmouth, <mtootkaboni@umassd.edu>

⁴ Professor, Department of Civil Engineering, Johns Hopkins University, <schafer@jhu.edu>

elements (i.e. webs, flanges, and lips) to the stresses developed over the cross-section elements under the combined actions. Particularly, local and distortional buckling of the cross-sections is directly tied to the stress distribution on the cross-section. Current cold-formed steel beam-column design does not determine stability under the actual combined actions, and ignores any nonlinear interaction in the strength between axial load and bending.

This paper numerically investigates the structural strength and stability of cold-formed steel Zee-section beam-columns under bi-axial moments and axial load. The modeling protocols required to predicted the strength of the Zee-section beam-columns are validated via a parametric study on the modeling parameters and comparison of the results against previously conducted experimental results. The modeling protocol can be used to complement the limited combination of experimentally investigated axial force and bi-axial bending moments and extend the test results to a complete strength surface to provide a more precise understanding of the structural behavior under combined actions. Moreover, the modeling protocol is the key to performing wider parametric analyses on different dimensions of Zee-sections under combined actions. The numerical results show the potential for improvements in the current specification approach, which utilizes a simple interaction equation for beam-column strength prediction.

The presented results are a part of an ongoing comprehensive study developing a new explicit DSM prediction for cold-formed steel beam-columns (Torabian et al. 2013). This larger effort includes tests on 600S137-54 lipped channel sections at a length of 610 mm [24 in.] and 1219 mm [48 in.] (Torabian et al. 2015) and also tests on cold-formed steel Zee sections (700Z225-60) at a length of 305 mm [12 in.] and 1219 mm [48 in.] (Torabian et al. 2016). In addition, complementary numerical analyses are also underway. The short length, 305mm [12 in.] specimens, considered here largely mobilize local modes of failures and thus this mode under combined actions is the primary focus of this paper.

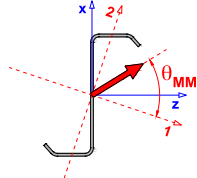
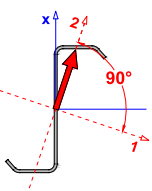
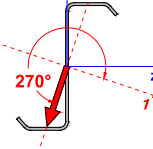
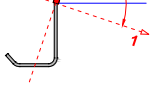
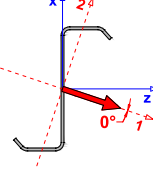
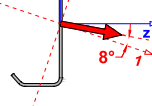
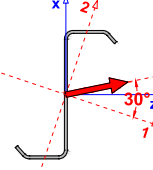
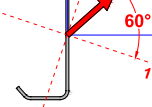
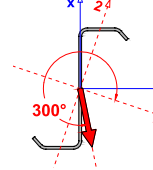
2. Experimental results

The experimental dataset used to validate the numerical models includes twenty-two Zee-section beam-columns with nominal 178 mm [7 in.] deep web, 57 mm [2.25 in.] wide flanges 19.5 mm [0.766 in.] long lips at 48 deg. and 1.52 mm [60 mil.] plate thickness. Inspired by the AISI designation for lipped channels, the Zee-section was given the nomenclature “700Z225-60” and tested at lengths of 305 mm [12 in.] and 1219 mm [48 in.] (see Torabian et al. 2016 for complete details). The cross-section was tested to explore beam-column performance under axial compressive load and any combination of major- and minor-axis bending. However, the number of points in the strength surface was limited to twenty. It was found that the cross-sectional applied stress distribution is the most important parameter in modulating the failure mechanisms, namely local or distortional buckling. In addition, the member ductility is strongly correlated to the degree of eccentricity in the applied axial load on the member (Torabian et al. 2016).

Table 1 summarizes the loading conditions and the peak load obtained in the experimental program. In this study, all tested specimens have been modeled and the names of the numerical models are consistent with the sequential number (first column in Table 1) of the specimens in the experiments. The loading conditions in Table 1 are in the normalized P - M_1 - M_2 coordinate. M_1 and M_2 are bending moments in the principal axes that are being normalized to the corresponding yield moments M_{1y} and M_{2y} , and denoted as x and y , respectively. The axial load is

also normalized to the yield load, P_y , and denoted as z . Each loading point in this non-dimensional cylindrical coordinate system is expressed using coordinates θ_{MM} and ϕ_{PM} , and β . θ_{MM} is an azimuth angle defined by $\tan^{-1}(y/x)$, ϕ_{PM} is an elevation angle $\cos^{-1}(z/\beta)$, and β is a radial length of $\sqrt{x^2 + y^2 + z^2}$ (see Torabian et al 2015 for more explanations on the P - M_1 - M_2 coordinate).

Table 1: Short beam-columns in the experimental program: L=305mm [12 in.]. (see Torabian et al. 2016)

Loading condition		θ_{MM} Target angle (deg.)	Test specimen Z700-12-	ϕ_{PM} Target angles (deg.)	θ_{MM-m} Measured angles (deg.)	ϕ_{PM-m} Measured angles (deg.)	P_u Peak load kN
No.							
1			1	25.0	277.1	24.0	109.8
2			2	50.0	277.3	49.3	92.8
3			3	81.0	277.0	81.3	37
4			22	81.0	277.0	81.0	32.3
5		Axial load and Minor axis bending	21 ^a	83	89.9	83.0	31.5
6			4 ^a	60	81.9	61.8	79.7
7			5 ^a	77	80.9	77.5	49.7
8			6 ^a	85	81.4	85.8	21.3
9			7	30.0	352.2	30.2	93.1
10		Axial load and Major axis/ Geometric Major axis bending	8	55.0	1.3	55.1	68.2
11			9	75.0	0.8	75.0	34.7
12			19 ^b	55.0	5.1	54.7	72.1
13			20 ^b	75.0	9.7	75.1	39.4
14		Axial load and Bi-axial bending	10	40.0	25.4	38.0	93.8
15			11	75.0	30.9	75.1	42.8
16			12	40.0	60.1	39.0	109.8
17			13	75.0	59.8	74.9	55.0
18			14	40.0	301.7	39.0	88.8
19			15	75.0	300.5	74.7	43.1
20			16	40.0	327.0	41.0	83.9
21		17	75.0	330.4	75.0	34.3	
22	Column		18	0.0	77.8	3.4	131.8

^a Due to the loading rig limitations, these specimens were tested upside-down.

^b Geometric Major axis ($\theta_{MM}=8$ deg.)

3. Numerical modeling

As shown in Table 1, the experimental program applies to only a limited number of P - M_1 - M_2 coordinate points on the strength interaction surface. To predict the entire strength interaction surface and also to understand the structural behavior of the beam-column more extensively,

geometric and material nonlinear shell finite element collapse analyses were performed in ABAQUS (Simulia, 2013). The models were validated using available experimental data to provide a viable modeling protocol. The modeling protocol includes material behavior, residual stresses and strains from cold-forming, geometric imperfections, cross-section dimensions, and boundary conditions. As described in the following sections, the imperfection pattern and magnitude are found to be the most important factors affecting the performance of the numerical models. To quantify these imperfection effects, a set of parametric analyses including different patterns and magnitudes of geometric imperfections were performed and the results were used to find the geometric imperfections to simulate short cold-formed steel Zee-section beam-columns most consistent with observations from testing.

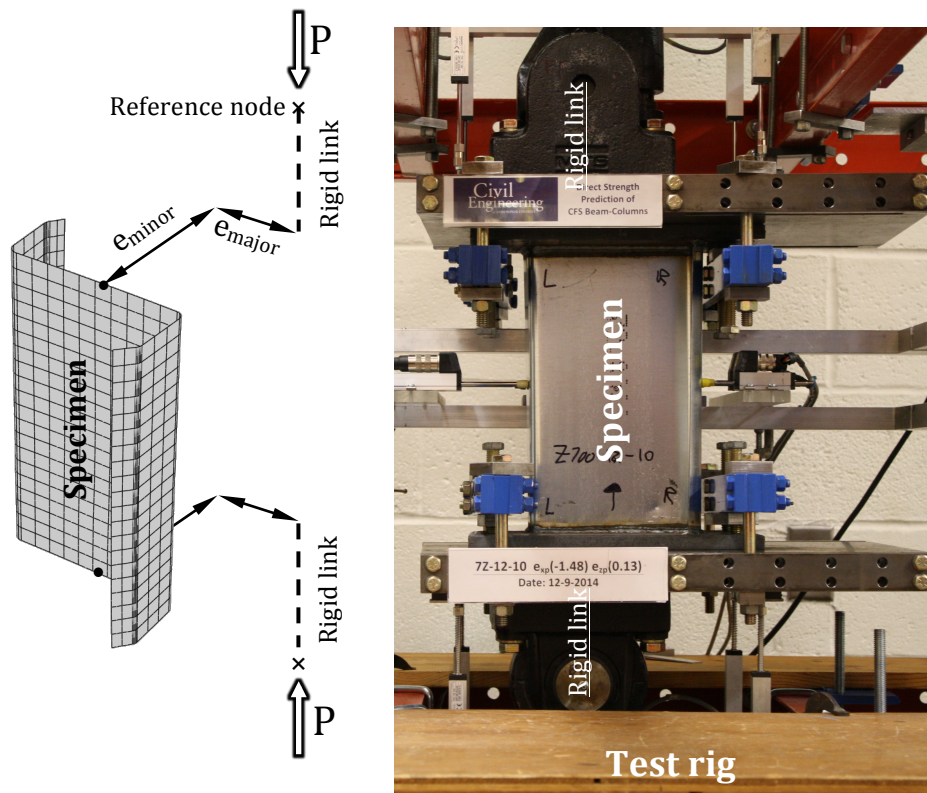


Figure 1: Finite element model: Geometric and boundary condition assumptions

3.1 Modeling assumptions

3.1.1 Model geometry and boundary conditions

Fig. 1 provides the general modeling assumptions including geometry and boundary conditions of the numerical model. Test specimens consisted of Zee-sections welded to 0.75 in. thick end plates. The endplates connected to the testing rig provided warping fixed restraints for the specimens. The end nodes of the specimen are constrained via an MPC-Beam constraint to the reference points placed at the location of swivel joints in the testing. The MPC-Beam constrains translations and rotational degrees of freedom (dofs) of all connected nodes to the reference node. The top reference node was restrained for all translations and torsional (rotations about longitudinal axis) dofs and the node is free to rotate about the other axes of rotation to mimic the pin boundary condition in the tests. The bottom reference node was also restrained against translational movements, other than the longitudinal direction. The reference points were placed

at the desired eccentricity consistent with the eccentricities measured in the experimental program after placing the specimen. The length of the rigid link between the reference point and the end of the specimen was 159 mm [6.25 inches] in the longitudinal direction. Axial force or displacement (based on the solver but typically force in this study) was applied at the bottom reference point in the longitudinal direction.

Both nominal and measured geometric dimensions have been considered for numerical analyses herein. The nominal dimensions of the Zee-section specimens are industry tabled values (BlueScope Buildings, 2010), as explained in Section 2. The realized cross-section dimensions of the test specimens such as depth (H), flange width (B), lip length (d) and the corner angles and radii were measured manually before testing. Three equally spaced longitudinal measurements were made for each specimen and the average dimensions of all specimens were implemented in the numerical models (see Torabian et al. (2016) for more details).

The ABAQUS shell element, S9R5, was utilized in the numerical models. This element has been shown to be more economical than other alternatives: S4, S4R and S8R5 (Schafer et. al. 2010). Based on a mesh density study shown in Table 2, an efficient mesh density including 10 elements in the web, 2 elements in the flange and the lip, 4 elements in the corner and 20 elements along the length were selected for the shell model (see Fig. 1).

Table 2: Mesh density studies on 12-inch long specimens subjected to axial compression

Mesh	Number of elements					CPU Time (sec.)	$\frac{P_{FEM}}{P_y}$
	Web	Flange	Lip	Corner	Longitudinal		
Fine	30	8	5	16	120	1671	0.32388
Medium 1	10	2	2	4	40	132	0.32468
Medium 2	10	2	2	4	20	68	0.32456
Coarse	2	1	1	2	20	44	0.33308

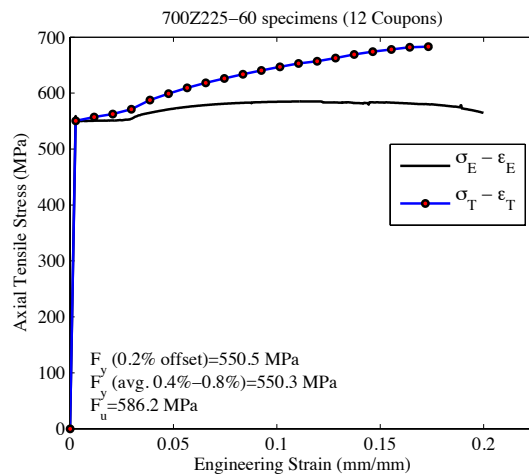


Figure 2: Engineering and true stress-strain curves for 12 coupons taken from Zee-section specimens

3.1.2 Material properties and residual stress and strain

The material properties are primarily based on the tensile testing results of 12 coupons taken from Zee-section specimens in the experimental program and converted to true stress-true strain. The plastic part of true stress-true strain curve shown in Fig. 2 was used to define material

properties in ABAQUS. The elastic Young’s modulus, the yield stress and the Poisson’s ratio were 2.03×10^5 MPa [29500 ksi], 550 MPa [80 ksi], and 0.3, respectively. The von Mises yield criteria, associated flow, and isotropic hardening were assumed for handling plasticity in the models. The distribution of the residual stresses and strains resulted from roll-forming were determined according to Moen et al. (2008), although more accurate distribution models could be adopted (see Amouzegar et al. (2015)). Only the residual stresses and effective plastic strains in the corner regions were considered and assigned to thirty-one through-thickness integration points in the finite element model.

3.1.3 Geometric imperfections

In geometric and material nonlinear shell finite element collapse analyses, geometric imperfections are key to producing realistic strength predictions (see Foroughi et al. (2014) and Amouzegar et al. (2015)). Signs, combinations, and magnitudes of the geometric imperfection patterns are all important and finding the best ensemble requires measurements and sensitivity analyses. Fig. 3 summarizes different potential uniform imperfection patterns resulting from buckling modes consistent with axial compression. As shown, for the local and distortional buckling modes, the sign of the imperfection may imply inward or outward flange or web deformations. Also, different signs of global imperfections can impose different local demands of the cross-section elements. As shown in Table 3, a parametric study considering a full combination of imperfection modes and signs (totally 8 cases) was performed to find the “best” imperfection pattern for modeling the Zee-sections. The imperfection cases are combined with two other conditions: with and without residual stresses and strains. Table 3 provides all studied combinations of the imperfection modes and signs along with the two roll-forming effect conditions.

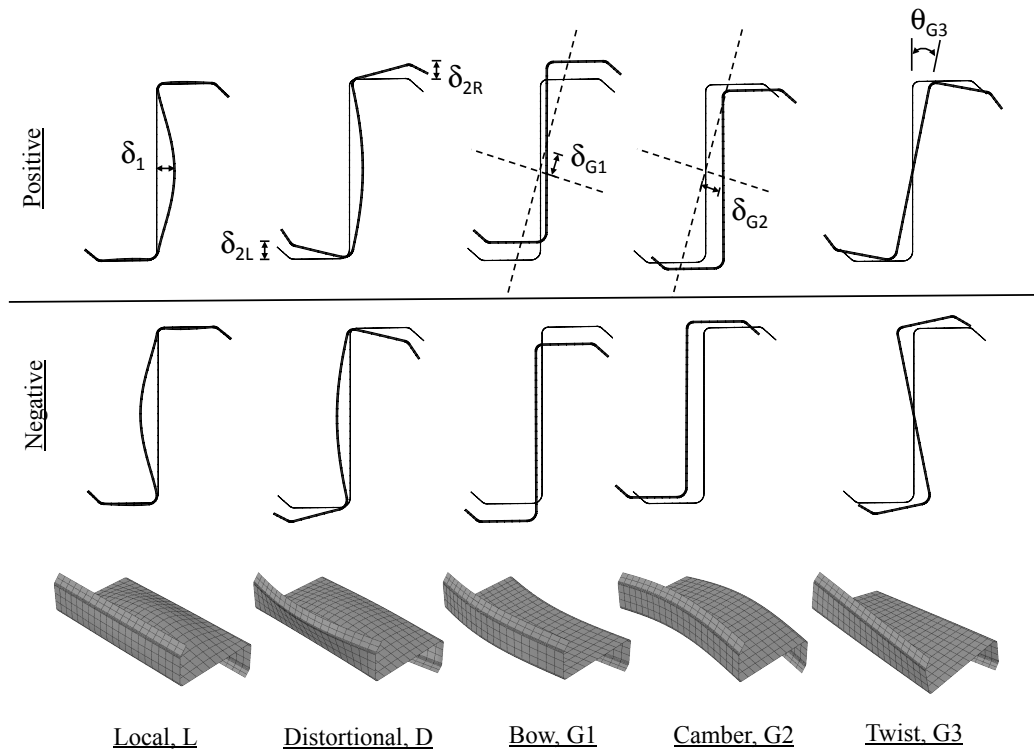


Figure 3: Typical buckling modes of Zee-sections in pure compression

Table 3: Combination of the imperfection patterns

Case No.	Designation	Imperfection mode						Residual stress and strain	
		Global, G1-G2-G3		Distortional, D		Local, L		With	Without
		(+)	(-)	(+)	(-)	(+)	(-)		
1	PGNDNL_N ^a	×			×		×		×
2	PGNDPL_N	×				×			×
3	PGPDNL_N	×		×			×		×
4	PGPDPL_N	×		×		×			×
5	NGNDNL_N		×		×		×		×
6	NGNDPL_N		×		×	×			×
7	NGPDNL_N		×	×			×		×
8	NGPDPL_N		×	×		×			×
9	PGNDNL_R ^a	×			×		×	×	
10	PGNDPL_R	×				×			×
11	PGPDNL_R	×		×			×		×
12	PGPDPL_R	×		×		×			×
13	NGNDNL_R		×		×		×		×
14	NGNDPL_R		×		×	×			×
15	NGPDNL_R		×	×			×		×
16	NGPDPL_R		×	×		×			×

^a P: Positive; N: Negative; _N: without residual stress and strains; _R: with residual stress and strain.

Table 4: Imperfection magnitude of different imperfection

Data set	Imperfection magnitude	Type I (Local) L	Type II (Distortional) D ^a		Bow G1	Camber G2	Twist G3	
		δ_1	δ_{2L}	δ_{2R}	δ_{G1}	δ_{G2}	θ_{G3}	
		(mm)	(mm)	(mm)	(mm)	(mm)	(deg)	
Zee-Section ^c	Zhao et al. (2015)	25%ile ^b	0.826	2.228	3.226	0.19	0.57	1.6
		50%ile	0.909	2.794	4.242	0.25	0.65	1.8
		75%ile	1.034	3.124	5.182	0.32	0.90	1.9
		95%ile	1.88	3.429	9.703	0.69	1.64	2.2
		99%ile	1.918	4.318	14.021	0.73	1.74	2.2
		Mean	1.046	2.725	5.123	0.30	0.82	1.7
		St. dev.	0.358	0.762	2.72	0.15	0.35	0.3
Lipped channel ^d	Zeinoddini and Schafer (2012)	25%ile	0.259	0.655	0.655	0.14	0.09	0.11
		50%ile	0.472	1.143	1.143	0.10	0.05	0.07
		75%ile	0.823	1.737	1.737	0.06	0.05	0.06
		95%ile	1.554	4.663	4.663	0.10	0.08	0.09
		99%ile	5.898	6.797	6.797	0.18	0.11	0.15
		Mean	0.716	1.570	1.570	0.36	0.21	0.26
St. dev.	0.945	1.478	1.478	0.40	0.25	0.29		

^a Maximum of δ_{2L} and δ_{2R} has been used in the numerical analyses.

^b Probability of exceedance (CDF values)

^c This dataset only includes measurements on the Zee-sections studied in the experiments.

^d Lipped channel dataset is across a large and broad set of Cee-sections

The magnitude of imperfections is a cross-section dependent quantity and actual measurements are required to determine its statistics. Zeinoddini and Schafer (2012) have studied the imperfection of lipped channel cross-section; and Zhao et al. (2015) have recently measured the imperfection of Zee-sections. Table 4 tabulates simple imperfection magnitudes corresponding to different probability of exceedance (CDF values) for simplified approximations of typical buckling shapes. These imperfection magnitudes were used in this study to validate the finite element model protocol (see Tables 5, and 6 for more details).

Table 5: Test-to-predicted ratios (P_{test}/P_{FEM}) for different imperfection patterns and measured geometric dimensions of the short specimens ($L=305\text{mm}$ [12 in.])

Imperfection magnitude from Zhao et al (2015) for 50%ile																
No.	Without residual stress and strain								With residual stress and strain							
	1	2	3	4	5	6	7	8	9	10	11	12	13	14	15	16
1	0.75	0.83	0.79	0.88	1.03	0.97	0.94	0.89	0.76	0.84	0.79	0.88	1.03	0.97	0.94	0.90
2	0.87	0.91	0.92	0.98	1.04	1.01	0.99	0.98	0.87	0.92	0.93	0.98	1.03	1.00	0.99	0.98
3	1.08	0.93	1.04	1.03	1.00	1.01	1.06	1.06	0.93	0.92	1.02	1.03	1.00	1.00	1.06	1.06
4	0.75	0.75	0.85	0.84	0.82	0.82	0.87	0.87	0.75	0.75	0.84	0.84	0.82	0.82	0.87	0.87
5	0.93	0.94	1.07	1.05	1.00	1.00	1.11	1.08	0.92	0.93	1.06	1.04	0.99	1.00	1.09	1.07
6	0.89	0.89	0.96	0.93	1.03	1.01	1.05	0.97	0.88	0.89	0.94	1.00	1.02	1.00	1.04	0.97
7	0.92	0.92	1.00	1.00	1.01	1.00	1.01	0.99	0.92	0.92	1.00	1.00	1.00	0.99	1.00	0.99
8	0.97	0.94	1.05	1.03	0.97	0.97	1.01	0.99	0.98	0.95	1.05	1.03	0.96	0.96	1.01	1.00
9	0.81	0.86	0.81	0.82	0.91	0.82	0.84	0.78	0.81	0.84	0.81	0.81	0.91	0.83	0.84	0.79
10	0.91	0.89	0.86	1.02	1.11	0.99	0.97	0.98	0.93	0.89	0.87	1.02	1.11	0.99	0.97	0.98
11	0.73	0.71	0.75	0.86	0.88	0.82	0.76	0.73	0.73	0.72	0.75	0.86	0.87	0.81	0.76	0.73
12	0.86	0.90	0.89	0.86	0.89	0.82	0.84	0.81	0.89	0.90	0.89	0.88	0.89	0.82	0.85	0.81
13	0.84	0.86	0.85	0.89	0.93	0.82	0.86	0.81	0.84	0.86	0.85	0.89	0.93	0.83	0.86	0.81
14	0.94	1.02	0.95	0.96	0.91	0.89	0.89	0.86	0.93	1.01	0.94	0.96	0.91	0.88	0.88	0.86
15	0.94	1.01	0.94	0.95	0.91	0.93	0.90	0.89	0.93	0.99	0.93	0.94	0.90	0.92	0.90	0.89
16	1.09	1.21	1.10	1.16	1.01	1.04	0.98	0.99	1.08	1.19	1.10	1.14	1.00	1.03	0.97	0.99
17	1.12	1.21	1.07	1.11	1.05	1.13	1.01	1.05	1.10	1.19	1.06	1.09	1.04	1.11	1.00	1.09
18	0.83	0.83	0.84	0.92	1.02	0.95	0.90	0.93	0.83	0.83	0.83	0.92	1.04	0.95	0.91	0.93
19	0.96	0.92	0.92	0.96	1.08	1.05	0.98	1.01	0.95	0.92	0.92	0.96	1.08	1.04	0.97	1.01
20	0.89	0.86	0.84	0.98	1.09	0.98	0.94	0.95	0.89	0.87	0.85	0.98	1.10	0.99	0.94	0.96
21	0.77	0.73	0.76	0.80	0.89	0.83	0.82	0.76	0.77	0.73	0.76	0.80	0.88	0.82	0.82	0.76
22	0.96	1.04	0.98	1.08	1.04	0.91	0.97	0.88	0.96	1.04	0.98	1.07	1.04	0.91	0.95	0.88
Avg.	0.90	0.92	0.92	0.96	0.98	0.94	0.94	0.92	0.89	0.91	0.92	0.96	0.98	0.94	0.94	0.92
St. dev.	0.11	0.13	0.11	0.10	0.08	0.09	0.09	0.10	0.10	0.12	0.10	0.09	0.08	0.09	0.08	0.10
Max.	1.12	1.21	1.10	1.16	1.11	1.13	1.11	1.08	1.10	1.19	1.10	1.14	1.11	1.11	1.09	1.09
Min.	0.73	0.71	0.75	0.80	0.82	0.82	0.76	0.73	0.73	0.72	0.75	0.80	0.82	0.81	0.76	0.73

3.2 Parametric studies and validation

The parametric study conducted here includes three imperfection magnitudes from Zhao et al. (2015) and four imperfection magnitudes from Zeinoddini and Schafer (2012). Each imperfection magnitude has been used to predict the strength of the Zee-section beam-columns for 8 different imperfection patterns and two different cases for considering roll-forming effects. The arc-length method (Riks) was selected to perform the 2464 total nonlinear shell finite element collapse analyses in ABAQUS, as summarized in Table 4 for imperfection magnitude of the 50%ile from Zhao et al. (2015), and also summarized in Table 5 for all imperfection magnitudes for two cases of imperfection patterns 13: NGNDNL_R, and 16: NGPDPL_R (see Table 3 for imperfection pattern nomenclature). Moreover, for imperfection patterns 13 and 16

and the imperfection magnitude from Zhao et al. (2015) for 50%ile, the test-to-predicted ratios have been provided for nominal geometric dimension in Table 6 to study the effect of geometric dimensions on the numerical predictions.

Based on the numerical results imperfection pattern 13: NGNDNL_R, which is negative global, distortional and local buckling shape (see Fig. 3) with included residual stresses and strains, provides the most consistent strength predictions (see Table 5 as an example). Comparing two different imperfection magnitudes shows that the Zhao et al. (2015) (50%ile), which are based on the studied Zee-sections, results in the closest prediction of strength in the numerical analyses, as shown in Table 6.

Table 6: A summary of parametric study results (P_{test}/P_{FEM}) on the imperfection magnitude and imperfection patterns of Zee-section test specimens

Data Set	Geometric dimensions	Imperfection pattern	Imperfection Magnitude	Test-to-predicted ratio (P_{test}/P_{FEM})					
				Mean	St. dev.	Max.	Min		
Zee-section Length=305 mm [12 in.]	Measured	13 NGNDNL_R	Zeinoddini and Schafer (2012)	99%ile	1.09	0.10	1.29	0.88	
				95%ile	0.96	0.08	1.09	0.81	
				75%ile	0.93	0.08	1.05	0.79	
				50%ile	0.92	0.08	1.03	0.77	
				95%ile	1.08	0.10	1.27	0.89	
	Nominal	13	Zhao et al. (2015)	50%ile	99%ile	1.04	0.09	1.19	0.90
					95%ile	0.94	0.09	1.06	0.78
					75%ile	0.92	0.10	1.13	0.72
					50%ile	0.91	0.11	1.14	0.70
					95%ile	0.91	0.09	1.06	0.75
Zee-section Length=305 mm [12 in.]	Measured	16 NGPDPL_R	Zhao et al. (2015)	75%ile	0.91	0.10	1.07	0.73	
				50%ile	0.92	0.10	1.09	0.73	
				95%ile	0.91	0.10	1.07	0.73	
				75%ile	0.91	0.10	1.07	0.73	
				50%ile	0.91	0.10	1.07	0.73	
Nominal	16	Zhao et al. (2015)	50%ile	99%ile	1.17	0.12	1.45	1.00	
				50%ile	1.17	0.12	1.45	1.00	

3.3 Failure modes

The observed failure modes in the numerical analyses and the recorded deformed shape of the tested specimens have been compared in Tables 7 for different loading conditions. As shown in the Table, the selected modeling protocol provided consistent simulated buckling shapes in the FEM analyses. Notably, the numerical results showed more symmetric buckling shapes, while the physical specimens often showed unsymmetrical modes of failure due to the actual imperfection patterns and irregularity in the specimens.

Table 7: Test results of the short specimens ($L=305\text{mm}$ [12 in.]): specimens at maximum strength and the cross-sectional deformation at mid-height. Numerical results based on the imperfection pattern 13: NGNDNL_R, imperfection magnitude from Zhao et al. (2015) for 50%ile, and measured geometric dimensions.

Spec. No. ^a	Axial force + Minor axis bending		Axial force + Major axis bending		Axial force + Bi-axial bending	
	(2)	(6)	(10)	(13)	(16)	(20)
Test Specimen at the failure load						
P_{\max} (kN)	92.8	79.7	68.2	39.4	109.8	83.9
Cross-section ^b deformation						
Numerical models at the failure load						
P_{FEM} (kN)	89.7	78.3	61.3	40.3	109.6	76.4

^a For specimen numbers and more details see Table 1.

^b blue: undeformed shape, cyan: $0.25P_{\max}$, green: $0.5P_{\max}$, yellow: $0.75P_{\max}$, red: P_{\max} , orange: $0.85P_{\max}$ -post peak.

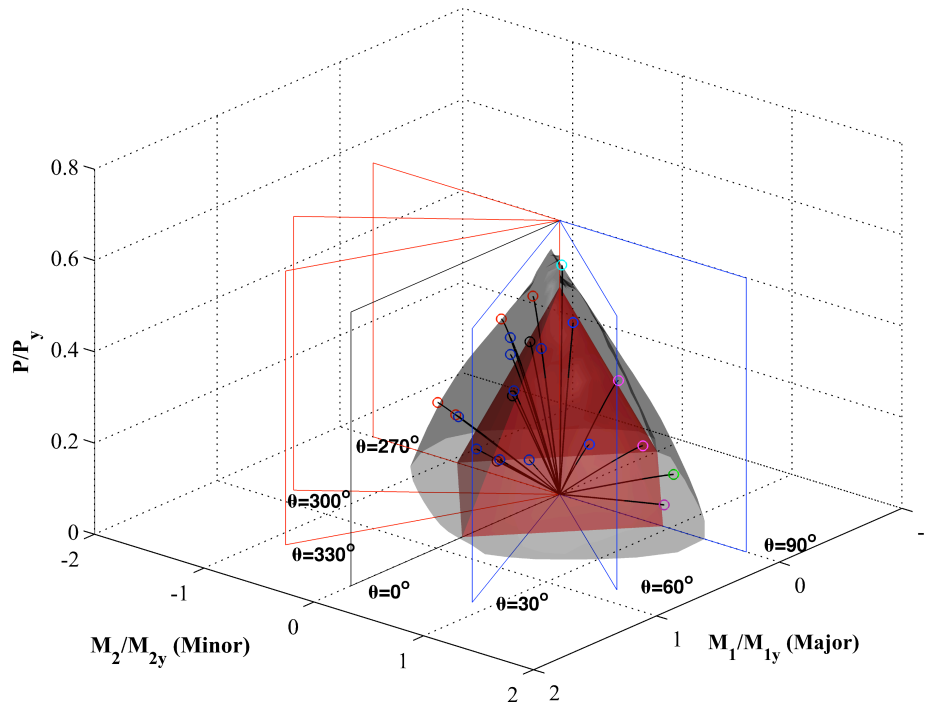


Figure 4: Strength surfaces in P - M_1 - M_2 space: Test results (lines and circles), linear interaction surface per AISI-S100-12 (red surface), FEM strength surface for the short Zee-section: 700Z225-60 (gray surface).

3.4 Strength interaction surface

The modeling protocol developed in the previous sections was implemented to construct a strength surface for the short Zee-section beam-column: 700Z225-60, L= 305mm [12 in.] The surface is based on the results of 704 collapse analyses with different eccentricities. The eccentricities were associated with 10° step in azimuth angle θ_{MM} and 5° step in the elevation angle ϕ_{PM} .

For comparison purposes, a linear interaction surface constructed based on the Direct Strength Method in AISI-S100-12 at the anchor points has been added to the strength interaction surface. As shown in the figure, the specification strength surface is completely inside the FEM strength surface (and the test results), thus showing that the specification provides conservative results for the entire P - M_1 - M_2 space. The specification predictions around the compression load anchor point and major axis bending anchor point provided the best results, while the minor axis bending predictions where the ($\theta_{MM}=90^\circ, 270^\circ$) show the most conservative prediction.

4. Summary and Conclusions

A series of material and geometric nonlinear collapse finite element analyses has been performed on a short Zee-section beam column (700Z225-60, L=305mm [12 in.]) using different imperfection patterns, imperfection magnitudes, residual stresses and strains, and geometric dimensions. The results are compared against the results of existing experiments on 21 short beam-columns to find an appropriate modeling protocol for numerical modeling of Zee-section beam-column. The selected modeling protocol consists of the following primary assumptions,

- S9R5 shell elements are used, with transverse discretization of: 10 elements in the web, 2 elements in the flange and the lip, and 4 elements in the corner. The element aspect ratio is kept close to one throughout the mesh.
- The von Mises yield criteria, associated flow, and isotropic hardening with a σ - ϵ curve based on direct experimental measurement were assumed for modeling plasticity in the numerical models.
- Roll-forming effects (residual stresses and strains) are considered for the corners of the cross-section based on the method set forth by Moen et al. (2008), but are not shown to have a significant effect on the results.
- Measured (as opposed to nominal) geometric dimensions are implemented in the modeling.
- An imperfection pattern consisting of sympathetic local and distortional modes along with global modes (which were small in this study) was selected. The selected pattern causes inward distortional buckling for the flange under compression, which is consistent with the test results.
- The imperfection magnitude was determined based on Zhao et al. (2015) measurements (50%ile), which were determined based on direct measurements of the Zee-sections. This imperfection magnitude is consistent with the large 95%ile imperfections on lipped channels from Zeinoddini and Schafer (2012).

After using the modeling protocol to construct the strength surface of the tested specimen, it was found that the current AISI-S100-12 specification predictions for the beam-column strength of this section (using DSM method for anchor points and interaction equations) are quite

conservative. The most conservative results were found to be under axial load and minor axis bending. The reserved capacity between the strength surfaces constructed by the AISI specification and the numerical interaction surface show the potential for improving the current specification methods for beam-column design. It should be noted that a new Direct Strength Method for beam-columns that directly incorporates stability under the actual applied P - M_1 - M_2 action and inelastic reserve in bending is underway and future improvements are desired.

Acknowledgments

The authors would like to acknowledge the American Iron and Steel Institute and the Metal Building Manufacturers Association for funding this study. The authors would also like to acknowledge the support of National Science Foundation under Grants No. CMMI-1235238 and CMMI-1351742. Any opinions, findings, and conclusions or recommendations expressed in this material are those of the authors and do not necessarily reflect the views of the sponsors or other participants.

References

- AISI-S100 (2012). "North American Specification for the design of cold-formed steel structural members." Washington (DC, USA): *American Iron and Steel Institute*.
- Amouzegar H., Amirzadeh B., Zhao X., Schafer B.W., Tootkaboni M. (2015), "Statistical Analysis of the Impact of Imperfection Modes on Collapse Behavior of Cold-Formed Steel Members", *Proceedings of Structural Stability Research Council Annual Stability Conference, Nashville, TN, March 24-27, 2015*.
- Amouzegar H., Schafer B.W., and Tootkaboni M. (2015). "An incremental numerical method for calculation of residual stresses and strains in cold-formed steel members". *Submitted to Thin-Walled Structures*.
- BlueScope Buildings. (2010) "Section properties for Zee Sections".
- Foroughi H., Moen C.D., Myers A.T., Tootkaboni M., Vieira L. and Schafer B.W. (2014), "Analysis and Design of Thin Metallic Shell Structural Members - Current Practice and Future Research Needs", *Proceedings of Structural Stability Research Council Annual Stability Conference, Toronto, Canada, March 25-28, 2014*.
- Li, Z., Schafer, B.W. (2010). "Application of the finite strip method in cold-formed steel member design." *Journal of Constructional Steel Research*, 66, 971–980.
- Moen, C.D., Igusa T., Schafer B.W. (2008). "Prediction of residual stresses and strains in cold-formed steel members", *Thin Wall Struct*, 46, 1274-1289.
- SFIA (2012). "Technical Guide for Cold-Formed Steel Framing Products." *Steel Framing Industry Association*
- Schafer, B.W., Li, Z., Moen, C.D. (2010). "Computational modeling of cold-formed steel." *Thin Wall Struct*, 48, 752-762.
- Simulia. (2013). ABAQUS 6.13. (www.Simulia.com).
- Standards Australia. (2005). "Cold-formed steel structures." NZS 4600, Sydney, Australia.
- Torabian S., Zheng B., Schafer B.W. (2013). "Direct Strength Prediction of Cold-Formed Steel Beam-Columns", *Thin-walled Structures Group at The Johns Hopkins University. American Iron and Steel Institute (AISI)*. (<http://www.ce.jhu.edu/bschafer/dsmbeamcol/>)
- Torabian, S., Fratamico, D. C., and Schafer, B. W. (2016). "Experimental response of cold-formed steel Zee-section beam-columns." *Thin-Walled Structures*, 98, 496–517.
- Torabian, S., Zheng, B., and Schafer, B. W. (2014). "Experimental study and modeling of cold-formed steel lipped channel stub beam-columns." *Proceedings of the Annual Stability Conference Structural Stability Research Council*, SSRC, Toronto, Canada, 21.
- Torabian, S., Zheng, B., and Schafer, B. W. (2015). "Experimental response of cold-formed steel lipped channel beam-columns." *Thin-Walled Structures*, Elsevier, 89, 152–168.
- Zeinoddini, V. M., Schafer, B.W. (2012). "Simulation of geometric imperfections in cold-formed steel members using spectral representation approach". *Thin-Walled Structures*, 60, 105–117.
- Zhao, X., Tootkaboni M., Schafer, B.W. (2015). "Laser-based Cross-Section Measurement of Cold-Formed Steel Members: Model Reconstruction and Application". *Submitted to Thin-Walled Structures*.